*Int. J. Heat Mass Transfer.* Vol. 25, No. 8, pp. 1183–1190, 1980
Printed in Great Britain

0017-9310/82/081183-08 $03.00/0


# BOUNDARY AND INERTIA EFFECTS ON CONVECTIVE MASS TRANSFER IN POROUS MEDIA

K. VAFAI* and C. L. TIEN
Department of Mechanical Engineering, University of California,
Berkeley, CA 94720, U.S.A.

(*Received* 18 *September* 1981 *and in final form* 4 *January* 1982)

**Abstract**—The present work consists of a numerical and experimental investigation of the effects of the presence of a solid boundary and inertial forces on mass transfer in porous media. Particular emphasis is placed on mass transfer through the porous medium near an impermeable boundary. The local volume-averaging technique has been used to establish the governing equations. The numerical solution of the governing equations is used to investigate the mass concentration field inside a porous medium close to an impermeable boundary. In conjunction with the numerical solution, a transient mass transfer experiment has been conducted to demonstrate the boundary and inertia effects on mass transfer. This is accomplished by measuring the time and space-averaged mass flux through a porous medium. The results clearly indicate the presence of these effects on mass transfer through porous media.

## NOMENCLATURE

$B$, blowing coefficient, $v_w/u_C$;
$Da$, Darcy number, $K/L^2$;
$D_{j,e}$, effective mass diffusion coefficient [$m^2\,s^{-1}$];
$F$, function used in expressing inertia terms in equation (13);
$K$, permeability of the porous structure [$m^2$];
$L$, horizontal extent of the external boundary [m];
$\dot{M}_j$, rate of production of species $j$ per unit volume [$kg\,m^{-3}\,s^{-1}$];
$m_j$, mass fraction of component $j$;
$\bar{m}_j$, dimensionless mass concentration, $(m_j - m_{j,eq})/(m_{j,\infty} - m_{j,eq})$;
$m_{j,eq}$, equilibrium mass concentration at the boundary;
$m_{j,\infty}$, free-stream mass concentration;
$P$, pressure [$N\,m^{-2}$];
$Re_m$, mass transfer Reynolds number, $\rho_e u_C L/\mu_f$;
$Sc_j$, effective Schmidt number, $\mu_f \delta/\rho_e D_{j,e}$;
$Sh_j$, Sherwood number defined in equation (17);
$\overline{Sh}_j$, time-averaged Sherwood number;
$\overline{\overline{Sh}}_j$, time and length-averaged Sherwood number, defined in equation (19);
$t$, time [s];
$\bar{t}$, dimensionless time, $t/(K/D_{j,e})$;
$u$, $x$-component velocity [$m\,s^{-1}$];
$u_C$, convective velocity, $-\frac{K}{\mu_f}\frac{dP}{dx}$ [$m\,s^{-1}$];
$\mathbf{V}$, velocity vector [m];
$v$, $y$-component velocity [$m\,s^{-1}$];
$v_w$, blowing velocity [$m\,s^{-1}$];
$x$, spatial coordinate, horizontal [m];
$y$, spatial coordinate, vertical [m].

Greek symbols

$\gamma$, porous media shape parameter, $(\delta/K)^{1/2}$ [$m^{-1}$];
$\delta$, porosity of the porous medium;
$\eta_j$, dimensionless vertical length scale, $y/(x/Sc_j Re_m Da^{1/2})$;
$\mu_f$, dynamic viscosity of the fluid [$kg\,m^{-1}\,s^{-1}$];
$\xi$, dimensionless horizontal length scale, $x/L$;
$\rho_e$, mass-averaged density $\sum_j \rho_j$ [$kg\,m^{-3}$];
$\rho_j$, density of species $j$ [$kg\,m^{-3}$];
$\Phi_j$, mass transfer boundary parameter, $(Sc_j/\gamma L)^2$;
$\Psi_m$, mass transfer inertia parameter, $F\delta^{3/2} Re_m/\gamma L$;
$\Omega_j$, blowing parameter for species $j$, $B\,Sc_j$.

Other symbols

$\langle\ \rangle$, denotes the "local volume-average" of a quantity.

## 1. INTRODUCTION

TRANSPORT phenomena in porous media have recently received considerable attention due to the increasing interest in geothermal operations, building thermal insulation, heat exchangers, petroleum reservoirs, chemical catalytic reactors and many other areas. This increase in the use of porous media has made it essential to find a better way of understanding the associated transport processes. However, the geometric complexity of the porous medium prevents exact solutions of the transport equations inside the

* Present address: Dept. of Mechanical Engineering, Ohio State University, Columbus, OH 43210, U.S.A.

pores. For this reason analytical simplifications must be introduced in analyzing transport phenomena in porous media. Most of the existing studies [1–4] deal primarily with the mathematical simplification based on Darcy's law, which neglects the effects of a solid boundary or the inertial forces on flow, heat and mass transfer through porous media. In many applications the porous medium is bounded and the fluid velocity is high. Therefore, it is important to investigate these boundary and inertia effects. In a previous paper [5] these effects on flow and heat transfer were analyzed and conveniently expressed in terms of three dimensionless parameters, which allowed a simple characterization scheme for interpreting the applicability of Darcy's law to various problems of flow and heat transfer in porous media. The present work discusses these effects on mass transfer through porous media. This includes a mass transfer experimental investigation to demonstrate the boundary and inertia effects. The study of mass transfer in porous media is essential due to its wide applications such as chemical catalytic reactors. An important difference between the heat and mass transfer processes lies in the function of the solid matrix. The solid matrix does not always participate in the mass transfer process as in the heat transfer case. In this regard, mass transfer can be analogous to a heat transfer process with zero solid-matrix thermal conductivity. This fact is especially useful in a mass transfer experiment since the properties of the solid-matrix are not needed.

The present analysis is concerned with transient mass transfer in porous media, in accordance with the experimental study which is transient in general. Indeed, many interesting features have been uncovered in the transient mass transfer analysis. The experimental measurements, which agree well with the numerical results, demonstrate in a convincing manner the boundary and inertia effects.

## 2. FORMULATION

The governing equations for mass transfer in porous media are developed here using the local volume-average technique [5–7]. This is done by associating with every point in the porous medium a small volume $V$ bounded by a closed surface $A$. Let $V_f$ be that portion of $V$ containing the fluid, and let $A_{sf}$ be the area of pore walls contained within $V_f$ as shown in Fig. 1. The local volume average of a quantity $\Psi$ associated with the fluid is then defined as

$$\langle \Psi \rangle \equiv \frac{1}{V} \int_{V_f} \psi \, dV. \tag{1}$$

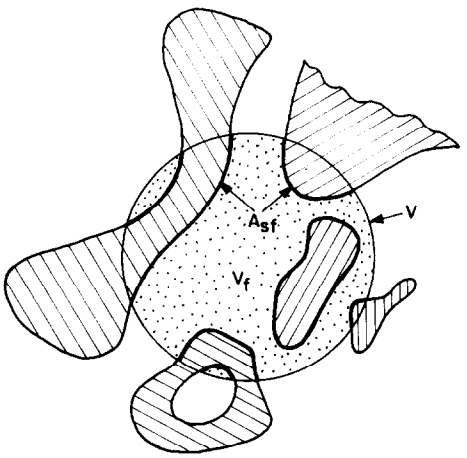


FIG. 1. The volume $V$ associated with every point in porous medium.

Using the "volume average of a divergence" theorem [6, 7], the local volume average of the mass, momentum and species equations for an incompressible, transient mass transfer through a porous medium with no body forces due to gravity, can be established as [5]

$$\nabla \cdot \langle \mathbf{V} \rangle = 0 \tag{2}$$

$$\rho_e \frac{\partial \langle \mathbf{V} \rangle}{\partial t} + \rho_e \langle (\mathbf{V} \cdot \nabla)\mathbf{V} \rangle = -\nabla \langle P \rangle + \mu_f \nabla^2 \langle \mathbf{V} \rangle + \mathbf{r} \tag{3}$$

$$\rho_e \frac{\partial \langle m_j \rangle}{\partial t} + \rho_e \langle \mathbf{V} \rangle \cdot \nabla \langle m_j \rangle = -\nabla \cdot \mathbf{\Lambda} + W + \langle \dot{M}_j \rangle \tag{4}$$

where

$$W = -\frac{1}{V} \int_{A_{sf}} (m_j \mathbf{V} - D_j \nabla m_j) \cdot d\mathbf{A} \tag{5}$$

$$\mathbf{r} = \frac{1}{V} \int_{A_{sf}} \mathbf{S} \cdot d\mathbf{A} \tag{6}$$

$$\mathbf{\Lambda} = \beta \nabla \langle m_j \rangle + \zeta |\nabla \langle m_j \rangle| \mathbf{V} \tag{7}$$

where the symbols are as defined in the Nomenclature, also $\mathbf{S}$ is the fluid's stress tensor, and $\beta$ and $\zeta$ complex functions of porosity $\delta$, $\rho_e$, $D_j$, $|\langle \mathbf{V} \rangle|$, $|\nabla \langle m_j \rangle|$ and $\langle \mathbf{V} \rangle \cdot \nabla \langle m_j \rangle$ [6]. Equations (2), (3) and (4) are 'macroscopic' conservation equations for fluid mass, momentum and species mass concentration, respectively. The body force term $\mathbf{r}$ is caused by the micropore structure, the rate of production term $W$ may result from a catalytic chemical reaction on the micropore structure and $\mathbf{\Lambda}$ can be considered as an effective mass flux vector of the porous medium and the fluid.

In the volume-averaging process some information is lost, thus requiring supplementary empirical relations for $\mathbf{r}$ and $\mathbf{\Lambda}$, as discussed in detail for the heat transfer part [5]. It should be noted that the empirical information to be employed here concerns specific physical terms in the fundamental transport equations and is quite different from the global empirical relations.

The effects of a solid boundary on flow and mass transfer in a porous medium originate from momentum diffusion caused by the boundary frictional resistance. This resistance is in addition to the bulk frictional drag induced by the solid matrix as characterized by Darcy's law. The boundary effects are best

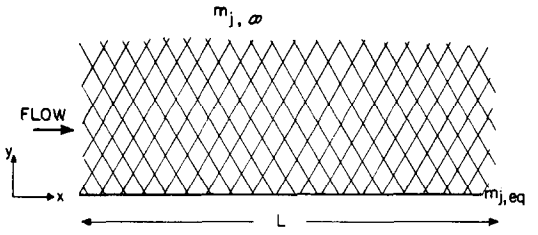


FIG. 2. Transient mass transfer in a porous medium confined by an external boundary.

described in terms of a new concept of the momentum boundary layer, in which the above two resistances are of the same order of magnitude. The procedure for arriving at the mass concentration boundary layer equations is similar to the heat transfer case [5] with two principal differences. First, variable natural blowing is present at the external boundary in the mass transfer case. This blowing is caused by the mass flux from the solid boundary to the fluid, which in turn causes a coupling between the velocity and mass concentration fields. Secondly, a rate of production by catalytic reaction may exist on the micropore structure represented by the term $W$ in the species equation (4).

*Two-dimensional transient mass transfer*

To illustrate the importance of the momentum boundary layer and its effects on mass transfer, an analysis is made for an incompressible, 2-dim. flow through a porous medium confined by an external boundary as shown in Fig. 2. An order of magnitude analysis of the species equation (4) indicates that the mass concentration boundary-layer thickness inside the momentum boundary layer is of the order of $(x/Sc_j\ Re_m Da^{1/2})$, where the symbols are as defined in the Nomenclature. This suggests the use of coordinate transformation so that convenient grid selection can be employed later to achieve efficient and accurate numerical computation of flow and mass concentration boundary layers. The governing momentum and species equations, (3) and (4) are then expressed as

$$\frac{1}{Sc_j\,\delta}\frac{\partial\langle\bar{u}\rangle}{\partial\bar{t}_j}+\Phi_j\frac{\Gamma_m^2}{\xi^2}\frac{\partial^2\langle\bar{u}\rangle}{\partial\eta_j^2}-\Psi_m\langle\bar{u}\rangle^2-\langle\bar{u}\rangle+1=0 \tag{8}$$

$$\frac{1}{\kappa_j\Gamma_m^2}\frac{\partial\langle\bar{m}_j\rangle}{\partial\bar{t}_j}+\xi^2\langle\bar{u}\rangle\frac{\partial\langle\bar{m}_j\rangle}{\partial\xi}-(\xi\eta_j\langle\bar{u}\rangle-\Omega_j\Gamma_m\xi)\frac{\partial\langle\bar{m}_j\rangle}{\partial\eta_j}=\kappa_j\Gamma_m^2\frac{\partial^2\langle\bar{m}_j\rangle}{\partial\eta_j^2}+\xi^2\bar{W}+\xi^2\langle\bar{M}_j\rangle \tag{9}$$

where

$$\xi=x/L,\ \eta_j=y/(x/Sc_j Re_m Da^{1/2}), \tag{10}$$

$$\bar{u}=u/u_C,\ m_j=(m_j-m_{j,eq})/(m_{j,\infty}-m_{j,eq}),\ \bar{t}_j=t/(K/D_{j,e}), \tag{11}$$

$$\bar{W}=W/(u_C(m_{j,\infty}-m_{j,eq})/L),\quad \bar{M}_j=\dot{M}_j/(\rho_e u_C(m_{j,\infty}-m_{j,eq})/L), \tag{12}$$

$$\Phi_j=(Sc_j/\gamma L)^2,\ \psi_m=F\delta^{3/2}Re_m/\gamma L,\quad \Omega_j=B\,Sc_j, \tag{13}$$

$$\kappa_j=Sc_j/Re_m,\ \Gamma_m=Re_m Da^{1/2}. \tag{14}$$

The function $F$ depends upon the Reynolds number, as well as the microstructure of the porous medium, and is related to the form drag caused by the porous matrix [5]. The given functional dependence of $F$ can be deduced from a number of empirical results [8, 9], which shows a weak dependence of $F$ on the Reynolds number.

The corresponding boundary conditions are

$$n_j=0,\quad \langle\bar{u}\rangle=0,$$

$$\langle\bar{v}\rangle=-D_{j,e}\frac{\partial\langle m_j\rangle}{\partial y}\bigg|_{y=0}\Big/(1-m_{j,eq})u_C, \tag{15}$$

$$\langle\bar{m}_j\rangle=0$$

$$\eta_j\to\infty,\ \langle\bar{u}\rangle=[-1+(1+4\Psi_m)^{1/2}]/2\Psi_m,\quad \langle\bar{m}_j\rangle=1 \tag{16}$$

where $v$ is the $y$-component velocity, and the boundary condition on $\bar{v}$ in equation (15) makes the velocity and mass concentration fields coupled.

The effects of the boundary on the velocity field are confined in a thin region and thus difficult to observe experimentally [5]. However, mass flux at the boundary, like the heat flux, a convenient quantity for experimental measurements, provides an indirect method with which to detect such effects. The Sherwood number, which characterizes the boundary mass flux, is expressed as

$$Sh_j=-\frac{\partial\langle m_j\rangle}{\partial y}\bigg|_{y=0}\Big/\frac{(m_{j,eq}-m_{j,\infty})}{L}=\frac{Sc_j}{\xi}\frac{\partial\langle\bar{m}_j\rangle}{\partial\eta_j}\bigg|_{\eta_j=0}. \tag{17}$$

In conducting the experiment, as explained in the next section, it is important to know the time interval within which steady-state conditions are effectively achieved. This is done by an order of magnitude analysis on the transient momentum and species equations (8) and (9). The former shows that the steady-state condition for the velocity distribution is reached within a time period of the order of $(K/\delta\nu_f)$, where $\nu_f$ is the kinematic viscosity. Physically this time corresponds only to a few seconds for most practical situations. Therefore, in the numerical analysis the steady-state form of the momentum equation (8) is considered. On the other hand, the order of magnitude analysis of the species equation reveals that the convective and diffusive mass transfer reach steady-state condition within time periods which are of the order of $(L/u_C)$ and $(K/D_{j,e})$, respectively. In physical situations these times correspond to several hundred

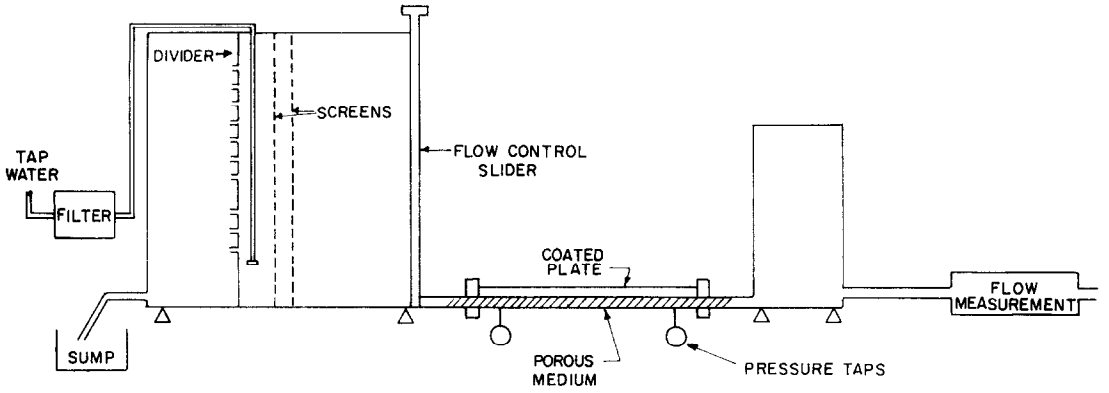


FIG. 3. Schematic diagram of experimental apparatus.

seconds. This is the reason for using the unsteady species equation (9) to obtain the numerical solutions. Furthermore, since there is neither a micropore catalytic reaction nor a global production of the species in the chosen experiment, both terms $W$ and $\dot{M}_j$ are set to be identically zero in equation (9). Setting $W$ equal to zero implies a non-participating porous matrix in the mass transfer case different from the heat transfer case.

### 3. EXPERIMENTAL APPARATUS AND TECHNIQUE

The apparatus employed to study the boundary and inertia effects on mass transfer through porous media is depicted schematically in Fig. 3. The set-up is designed to provide accurate flow and mass flux measurements. The purpose of the experiment is to obtain the average mass flux rate of a sucrose-coated plate to the water flowing through a test section filled with a porous medium. This is then compared with the mass flux rate obtained from the numerical solution.

The test section (30 × 10 × 1 cm; length, width and height, respectively) has two pressure taps connected to a U-tube manometer which uses a 1.75 specific gravity fluid. A porous block is located inside the test section pictured in Fig. 4. The upper portion of the test section is removable so as to accommodate the sucrose-coated plate on top of the porous medium. The high solubility of sucrose in water prevents the sucrose from being trapped in the porous matrix. The porous medium used is Foametal, a high-permeability medium used extensively in industrial applications such as heat exchangers, chemical reactors and fluid filters. Upstream of the test section is a reservoir capable of achieving a range of accurately designated levels. This is done through its connection via a divider

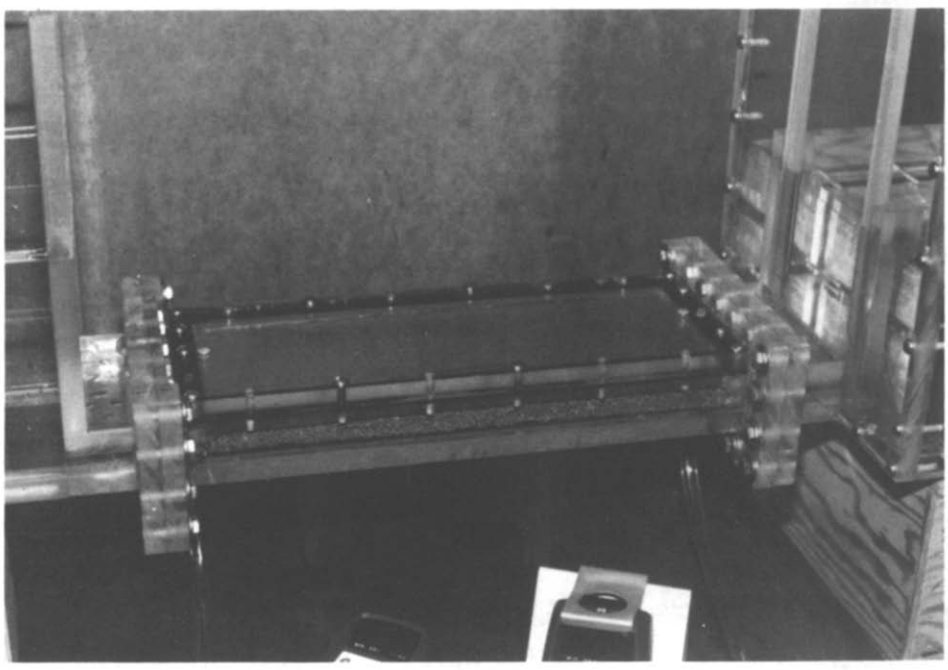

FIG. 4. Photograph showing the test section.

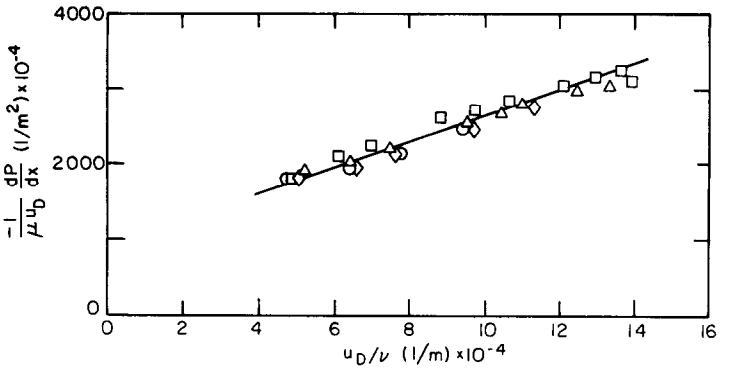


FIG. 5. Experimental results used in determining the permeability and the function $F$ of the Foametal.

to an auxiliary tank connected to the sump. Water enters the reservoir (25 × 25 × 40 cm) through a variable flow rate filter. Two mesh screens installed in the reservoir reduce any disturbances in the water before entering the test section. This disturbance-reduction effect is further enhanced by the extended portion of the porous medium before the test section. A highly accurate flow control slider disconnects the reservoir from the test section. The slider allows steady-state operating conditions upstream of the test section to be achieved before any fluid flows through it. This design, coupled with the large reservoir capacity, allows steady flow conditions to be obtained within seconds of the slider being opened, as seen from the pressure indicator and water levels in the upstream and downstream reservoirs.

The downstream reservoir (12 × 12 × 25 cm) is used to maintain a constant pressure difference at every height along the test section. It is connected to a trapezoidal section enabling finely controlled flow measurements through its small square outlet. The average mass flux rate is obtained by taking solution samples from the trapezoidal section. This is done after a small lapse to achieve steady flow.

## 4. RESULTS AND DISCUSSION

The permeability and the function $F$ which depends on the microstructure of the Foametal used in the experiment have to be determined prior to the mass transfer experiment. This is done by doing flow measurements at different pressure differences across the test section. At each pressure difference the average of three or four flow rate readings were taken. The results of these measurements are shown in Fig. 5. The velocity $u_D$ in Fig. 5 is given by the following equation:

$$\frac{dP}{dx} = \frac{-\mu_f}{K}u_D - \frac{F(K, \text{Geometry})}{K^{1/2}}\rho_f u_D^2 \qquad (18)$$

where $\rho_f$ is the fluid density. From this figure and equation (18) the permeability of the porous medium is found to be $1.11 \times 10^{-7}$ m$^2$, and $F$ to be 0.057. In calculating the permeability and the function $F$ from equation (18), we have implicitly neglected the effect of the solid boundary on the overall flow rates. This is a good approximation since the momentum boundary layer is confined to a thin region compared to the total flow cross section.

The experimental runs were made at different pressure differences across the test section. Table 1 presents the pressure gradients in terms of (N m$^{-3}$) across the test section. Included also are the times during which the samples were taken. The sucrose concentration of the samples was obtained by an acid hydrolysis giving an accurate count of the sucrose in the solution.

Table 1. Physical data for different experimental runs

| Experimental run | Pressure gradient (N m$^{-3}$) | Starting time (s) | Duration time (s) | $\Phi_j$ | $\Psi_m$ | Time and length-averaged Sherwood number |
|---|---|---|---|---|---|---|
| 1 | 232 | 5 | 20 | 4.61 | 0.38 | 990 |
| 2 | 349 | 25 | 25 | 4.61 | 0.58 | 1012 |
| 3 | 436 | 25 | 25 | 4.61 | 0.72 | 1103 |
| 4 | 639 | 25 | 25 | 4.61 | 1.0 | 1290 |
| 5 | 406 | 15 | 25 | 4.61 | 0.674 | 456 |
| 6 | 1046 | 25 | 25 | 4.61 | 1.73 | 1067 |
| 7 | 221 | 25 | 30 | 4.61 | 0.366 | 730 |
| 8 | 290 | 25 | 30 | 4.61 | 0.481 | 749 |
| 9 | 523 | 20 | 20 | 4.61 | 0.867 | 930 |
| 10 | 360 | 20 | 20 | 4.61 | 0.597 | 730 |

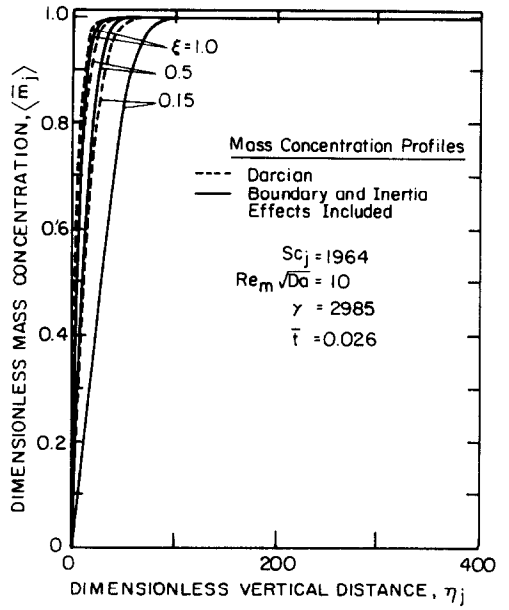


FIG. 6. The non-dimensional mass concentration profiles for the time $\bar{t} = 0.026$, corresponding to the second run.

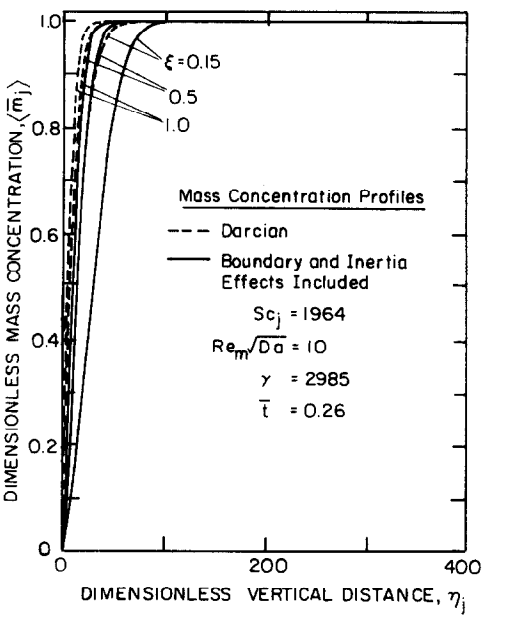


FIG. 8. The non-dimensional mass concentration profiles for the time $\bar{t} = 0.26$, corresponding to the second run.

The mass concentration fields for the second experimental run were computed numerically and are presented in Figs. 6–8. The numerical scheme is based on the steady-state linearized version of equation (8), using upwind differencing in the $\xi$-direction, an implicit routine in the $\eta_j$-direction, and an explicit marching routine in time. The linearization scheme for equation (8) has been checked by increasing the number of iterations used for convergence. Since equation (9) is coupled to the vertical velocity at the wall by the boundary condition (15), an iterative approach is used in solving equation (9). For a given time and longitudinal position, equation (9) is iterated until the value for the vertical velocity at the boundary converges. This value is then used in the final iteration of equation (9) to obtain the mass concentration distribution. The accuracy of the finite-difference solution has been tested through increasing the number of grid points. The Darcian profiles correspond to when boundary and inertia effects are neglected. Comparing Figs. 6–8, showing the mass concentration fields at three different times during the experiment, the approach towards steady-state becomes evident. The corresponding time averaged Sherwood numbers along the test section are presented in Fig. 9. Figure 9 shows that when boundary and inertia effects are

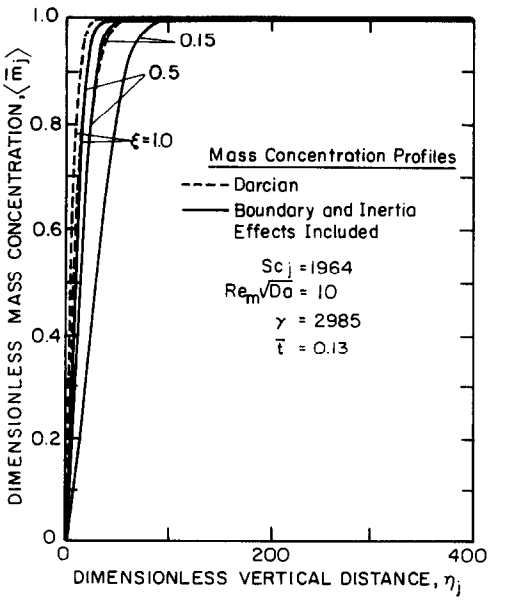


FIG. 7. The non-dimensional mass concentration profiles for the time $\bar{t} = 0.13$, corresponding to the second run.

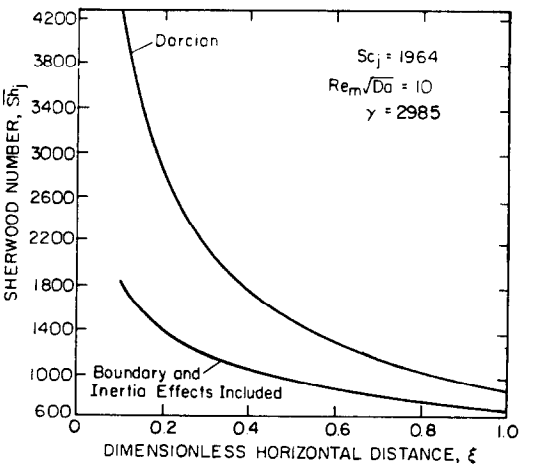


FIG. 9. Comparison of the time-averaged Sherwood numbers for the two cases presented in Figs. 6–8.

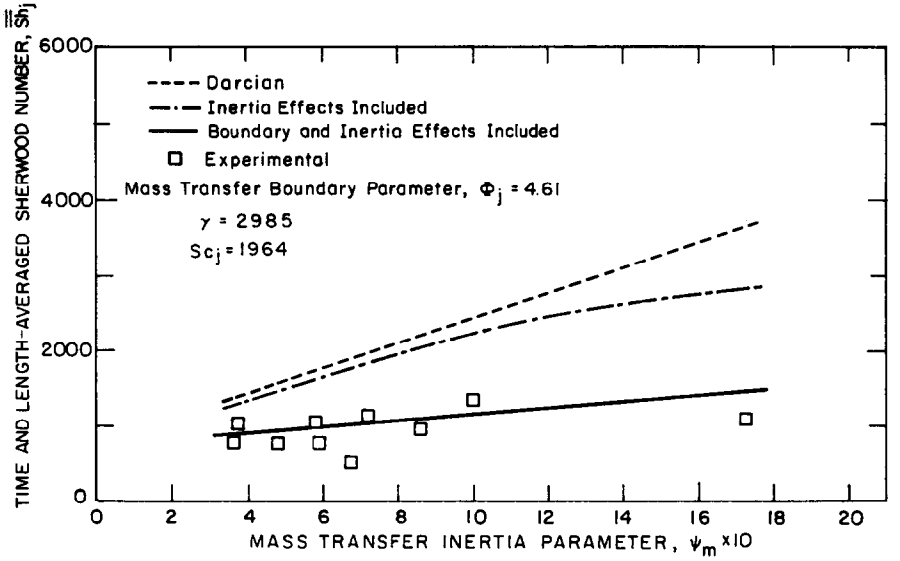


FIG. 10. Comparison of numerical and experimental Sherwood numbers.

included, lower mass flux rates are obtained than when these effects are not included. This is because of the higher velocities, close to the boundary, used in computing the mass flux rates when these effects are not included.

A time and length-averaged Sherwood number over a time period $t_f$ is defined as

$$\overline{\overline{Sh_j}} = \frac{1}{t_f L}\int_{t_s}^{t_s+t_f}\int_{L_s}^{L_s+L} Sh_j \, dx \, dt \qquad (19)$$

where $t_s$ and $L_s$ denote the time and length when the experiment started. The time and length-averaged Sherwood number for the mass transfer experiments are presented in Fig. 10. Included also are the numerical results for the three cases corresponding to the different velocity profiles used in computing the Sherwood numbers. These are the Darcian velocity profile, the velocity profile which includes only the inertia effects, and the velocity profile which includes both boundary and inertia effects. The parameter $\Psi_m$ in Fig. 10 is related to the pressure difference across the test section. The higher the pressure difference, the higher the inertia parameter $\Psi_m$. The Sherwood number $Sh_j$ relates to the time and length-averaged mass flux from the coated plate. The boundary parameter $\Phi_j$ is a measure of the boundary effects for a given porous medium, fluid and species $j$. The value of $\Phi_j$ for the experimental set-up used was 4.61. As shown in Fig. 10, higher pressure differences across the test section result in larger mass flux rates from the coated plate. It can be seen that at smaller values of $\Psi_m$, the case which accounts only for the inertia effects is quite close to the case which uses a Darcian velocity profile. However, as the value of $\Psi_m$ increases it causes a significant difference between the two cases. This is due to the velocity-squared correction term in the inertia-included case which is small at lower values of $\Psi_m$. At larger values of $\Psi_m$ this term becomes important due to the increase in the form drag resistance at higher velocities. In the limit of no flow across the test section ($\Psi_m = 0$), the Sherwood numbers obtained for the three numerical cases, shown in Fig. 10, converge to one value corresponding to the diffusion mass flux from the coated plate in the absence of convection.

It can be seen from Fig. 10 that the experimental data is in better agreement with the numerical results which include boundary and inertia effects. The significance of these results can also be extended to heat transfer in a porous medium, because of the analogies which exist between heat and mass transfer.

## 5. CONCLUSIONS

The purpose of this work was to investigate the significance and importance of the boundary and inertia effects on mass transfer in porous media. This has been done both numerically and experimentally. First, the general formulation of the problem is presented and then applied to the specific case of 2-dim. flow through porous medium confined by an external boundary. In doing so, the coupling between the velocity and mass concentration fields is demonstrated. An experimental set-up is then used to obtain mass transfer results for comparison with a numerical analysis which includes the effects of boundary and inertia in one case and excludes them in another. The results clearly show the importance of these effects on mass transfer through porous media.

## REFERENCES

1. A. E. Scheidegger, *The Physics of Flow through Porous Media*. University of Toronto Press, Toronto (1974).
2. P. C. Carman, *Flow of Gases through Porous Media*. Academic Press, New York (1956).

3. R. E. Collins, *Flow of Fluids through Porous Materials*. Reinhold, New York (1961).
4. M. Muskat, *The Flow of Homogeneous Fluids through Porous Media*. Edwards, Michigan (1946).
5. K. Vafai and C. L. Tien, Boundary and inertia effects on flow and heat transfer in porous media, *Int. J. Heat Mass Transfer* **24**, 195–203 (1981).
6. J. C. Slattery, *Momentum, Energy and Mass Transfer in Continua*. Krieger, New York (1978).
7. S. Whitaker, Advances in theory of fluid motion in porous media, *Ind. Engng Chem.* **61**, 14–28 (1969).
8. G. S. Beavers and E. M. Sparrow, Non-Darcy flow through fibrous porous media, *J. Appl. Mech.* **36**, 711–714 (1969).
9. J. C. Koh, J. C. Dutton, B. A. Benson and A. Fortini, Friction factor for isothermal and non-isothermal flow through porous media, *Trans. Am. Soc. Mech. Engrs*, Series C, *J. Heat Transfer* **99**, 367–373 (1977).

## EFFETS DE FRONTIERE ET D'INERTIE SUR LA CONVECTION MASSIQUE DANS LES MILIEUX POREUX

**Résumé**—L'article concerne une étude numérique et expérimentale des effets de la présence d'une frontière solide et des forces d'inertie sur le transfert massique dans les milieux poreux. Une importance particulière et portée sur le transfert massique à travers le milieu poreux au voisinage d'une frontière imperméable. La technique de la moyenne locale en volume est utilisée pour établir les équations de base. Leur solution numérique est utilisée pour étudier le champ de concentration massique près d'une frontière imperméable. En parallèle, une expérimentation est conduite pour montrer les effets de frontière et d'inertie sur le transfert massique par la mesure du flux massique, moyen dans le temps et dans l'espace, à travers un milieu poreux. Ce résultat montre clairement la présence de ces effets.

## RAND- UND TRÄGHEITSEINFLUSSE BEIM KONVEKTIVEN STOFFTRANSPORT IN PORÖSEN MEDIEN

**Zusammenfassung**—In dieser Arbeit wurden die Einflüsse einer festen Berandung und von Trägheitskräften beim Stofftransport in porösen Medien numerisch und experimentell untersucht. Besonderes Gewicht wird auf den Stofftransport durch poröse Medien an einer undurchlässigen Berandung gelegt. Zur Herleitung der Grundgleichungen wurde das Verfahren örtlicher volumetrischer Mittelwertsbildung angewandt. Die numerische Lösung der Grundgleichungen wurde verwendet, um das Massenkonzentrationsfeld in einem porösen Medium in der Nähe einer undurchlässigen Wand zu untersuchen. In Verbindung mit der numerischen Lösung wurde ein instationäres Experiment zur Demonstration der Rand- und Trägheitseinflüsse auf den Stofftransport durchgeführt. Dies wurde durch Messung des zeitlich und räumlich gemittelten Massenstroms in dem porösen Medium erreicht. Die Ergebnisse zeigen deutlich die vorhandenen Einflüsse auf den Strofftransport in porösen Medien.

## ВЛИЯНИЕ ГРАНИЧНЫХ УСЛОВИЙ И ИНЕРЦИОННЫХ СИЛ НА КОНВЕКТИВНЫЙ МАССОПЕРЕНОС В ПОРИСТЫХ СРЕДАХ

**Аннотация** — Представлено численное и экспериментальное исследование влияния твердой границы и сил инерции на массоперенос в пористых средах. Особое внимание обращено на массоперенос в пористой среде вблизи непроницаемой границы. Метод локального усреднения по объему использовался для вывода уравнений, численное решение которых позволило определить поле концентраций внутри пористой среды вблизи непроницаемой границы. Проведен также эксперимент с целью выяснения влияния границы и сил инерции на нестационарный массоперенос, при этом измерялись время и усредненный по пространству поток массы через пористую среду. Результаты свидетельствуют о влиянии указанных факторов на массоперенос в пористых средах.